



Fallon, E. K., Niehorster, E., Brooker, R. A., & Scott, T. B. (2018). Experimental leaching of massive sulphide from TAG active hydrothermal mound and implications for seafloor mining. *Marine Pollution Bulletin*, 126, 501-515. <https://doi.org/10.1016/j.marpolbul.2017.10.079>

Peer reviewed version

License (if available):  
CC BY-NC-ND

Link to published version (if available):  
[10.1016/j.marpolbul.2017.10.079](https://doi.org/10.1016/j.marpolbul.2017.10.079)

[Link to publication record in Explore Bristol Research](#)  
PDF-document

This is the author accepted manuscript (AAM). The final published version (version of record) is available online via ELSEVIER at <https://www.sciencedirect.com/science/article/pii/S0025326X17309256?via%3Dihub>. Please refer to any applicable terms of use of the publisher.

## University of Bristol - Explore Bristol Research

### General rights

This document is made available in accordance with publisher policies. Please cite only the published version using the reference above. Full terms of use are available:  
<http://www.bristol.ac.uk/pure/about/ebr-terms>

# 1 **Experimental leaching of sulphide ore from TAG hydrothermal mound and implications** 2 **for seafloor massive sulphide mining**

3  
4 **Emily K Fallon**<sup>1,2</sup>, Ella Niehorster<sup>1</sup>, Richard A Brooker<sup>2</sup>, Thomas B Scott<sup>1</sup>,

5 <sup>1</sup> Interface Analysis Centre, School of Physics, HH Wills Physics Laboratory, Tyndall Ave. University of Bristol, BS8  
6 1TL. UK.

7 <sup>2</sup> School of Earth Sciences, Wills Memorial Building, Queens Rd, University of Bristol, BS8 1RJ. UK.  
8

9 \*Current address to which correspondence should be sent; Interface Analysis Centre, School of Physics, HH Wills  
10 Physics Laboratory, Tyndall Ave. University of Bristol, BS8 1TL. UK.

11 Tel. (44) 117 3317685

12 Email. [e.fallon@bristol.ac.uk](mailto:e.fallon@bristol.ac.uk)  
13

## 14 **Abstract**

15 Seafloor massive sulphide (SMS) samples from the Trans-Atlantic Geotraverse deposit on the Mid-Atlantic Ridge  
16 were characterised and subjected to leaching experiments to emulate proposed SMS mining processes. Over  
17 time, leached Fe is removed from solution by the precipitation of Fe oxy-hydroxides, whereas Cu and Pb leached  
18 remained in solution at ppb levels. Bulk chemistry is not the main control on leachate concentrations; instead  
19 mineralogy and/or galvanic couples between minerals are the driving forces behind the type and concentration of  
20 leached metals. Dissolved concentrations exceed ANZECC toxicity guidelines by 620 times, implying the formation  
21 of localised toxicity in a stagnant water column. Moreover, concentrations will be higher when scaled to higher  
22 rock-fluid ratios and finer grain sizes proposed for mining scenarios. The distance at which dilution is achieved to  
23 meet guidelines is unlikely to be sufficient, indicating a need for the refinement of the mining process.

## 24 **Keywords**

25 SMS deposits

26 Mining impact

27 Leaching

28 Metal release

29 Toxicity  
30

## 31 **1 Introduction**

32 As the global demand for metals continues to grow, driven by advances in technology, so does the market price.

33 With the majority of economically viable terrestrial resources already exploited and fewer being discovered,

34 previously disregarded sources of metals are now beginning to be more seriously considered. Heightened interest

35 in seafloor exploration is highlighted by governments and commercial enterprises already applying for and

36 receiving licenses for exploration, with 26 exploration licences issued by the International Seabed Authority (ISA)

37 as of July 2015, covering 1.2 million square kilometres of the seafloor ((ISA), 2016). Additionally, there are an  
38 estimated 26 exploration projects within national jurisdiction areas of individual states' economic exclusion zones  
39 (EEZs) (ECORYS, 2014). Further to this, 77 submissions have been made by 67 different territories to extend their  
40 continental shelf and subsequently their economic exclusion zone to lay claim to larger expanses of the seafloor  
41 and associated mineral resources ((CLCS), 2016). Advances in deep-sea oil and gas extraction technology have  
42 paved the way for the economic viability of deep-sea mining. As a result, expectations are high that this industry is  
43 about to emerge.

44

45 Seafloor massive sulphide (SMS) ore deposits and their economic worth has been discussed extensively in the  
46 literature (German et al., 2016; Hannington and Jamieson, 2011; Hannington et al., 2010; Monecke et al., 2016),  
47 with Nautilus Minerals Inc. already in the process of commencing mineral extraction in what would be the world's  
48 first SMS mine at the Solwara 1 deposit in the Bismarck Sea off Papua New Guinea. In order to support any future  
49 economic potential, our knowledge and understanding of such deposits requires significant improvement with an  
50 associated need for assessment of any environmental impact that any future endeavours may produce.

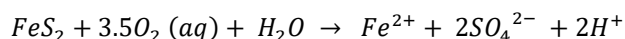
51

52 Sulphide minerals at both active and inactive hydrothermal seafloor vents undergo chemical interaction with  
53 seawater. This generally results in oxidative weathering (Edwards, 2004a), a process similar to the weathering that  
54 occurs in their terrestrial counterparts – volcanogenic massive sulphide (VMS) deposits. On land in restricted  
55 drainage systems, this occurs more vigorously at decreasing values of pH and can result in acid mine drainage  
56 (AMD), which promotes further dissolution as shown for pyrite in Eq. 1 & 2.

57

#### 58 Equation 1

59

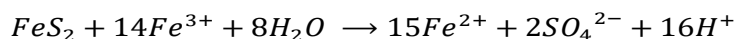


60

61

#### 62 Equation 2

63

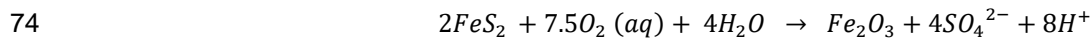


64

65 In contrast, this equivalent weathering process on the seafloor occurs in waters of near neutral pH and of almost  
66 'infinite' volume, so that arising acidity from oxidation is almost immediately buffered and low pH conditions will not  
67 develop over a significant area due to the dilution effect. The reactions result in formation of insoluble oxy-  
68 hydroxide minerals such as goethite and hematite at the expense of sulphides such as pyrite; as illustrated in Eq.  
69 3 & 4 (Mills and Elderfield, 1995; Edwards, 2004). These Fe oxide minerals can accumulate as crusts or caps on  
70 sulphide deposits on the seafloor and are referred to as 'gossans' with the mineral mixtures often referred to as  
71 limonite (Herzig and Hannington, 1995).

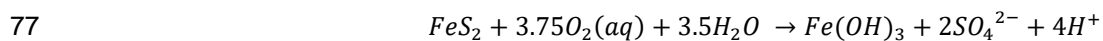
72

73 **Equation 3**



75

76 **Equation 4**



78

79

80

81 Based on the natural seafloor weathering process, it is argued that any exposure of sulphide as a result of mining  
82 will have a similar effect: with negligible net release of metals and pH that is buffered to neutral. However, the  
83 process of deep-sea mining has the potential to expose a high surface area of fresh sulphide minerals to the  
84 corrosive effects of seawater, allowing for an anthropogenic leaching of metals that is more akin to acid mine  
85 drainage observed in a terrestrial setting (Gwyther, 2008; Parry, 2008; Simpson et al., 2007). The only current  
86 concept for SMS mining is provided by Nautilus Minerals Inc. and includes an 'in situ' extraction phase that  
87 produces 80% <25mm and 20% smaller unknown particle size material, (where 30% of cut material is initially lost  
88 and up to 10% will remain on the seafloor). This is combined with a dewatering process that occurs as the mineral  
89 slurry (1:9 rock to fluid ratio) is carried to the surface, processed above sea level, and the waste water is returned  
90 to 25 to 50 m above the seafloor containing <8 µm sulphide particles at 6.35 g/L rock to fluid ratio. Both 'in situ'  
91 extraction and dewatering involve the entrainment of fresh sulphide material into an advective environment, with  
92 the dewatering process also providing exposure of sulphide to warmer temperature at the sea surface.

93

94 If any leaching of metals is not balanced by precipitation of oxides, there is the potential for local accumulation of  
95 dissolved heavy metals in the water column. These metals may bio accumulate in local ecosystems, disperse or  
96 accumulate in the wider ocean or ultimately precipitate elsewhere as oxides. As SMS deposits have been around  
97 for most of the Earth's history, it might be assumed there is equilibrium established between weathering processes  
98 and the local bio-environment. However, the natural weathering process has the potential to be locally  
99 exaggerated by any future mining of SMS deposits and exposure of significant fresh surface area.

100

101 The majority of previous dissolution studies are related to terrestrial acid mine drainage arising from mine flooding  
102 and leaching of tailings piles by meteoric waters (Acero et al., 2009; Bonnissel-Gissingner et al., 1998; Constantin  
103 and Chiriță, 2013; Descostes et al., 2004; Kwong et al., 2003; McKibben and Barnes, 1986; Moses et al., 1987). A  
104 small number of dissolution studies of specific sulphide minerals in seawater have been undertaken (Bilenker,  
105 2011; Bilenker et al., 2016; Feely et al., 1987; Romano, 2012) and demonstrate the large difference in oxidation  
106 rates between different sulphide minerals, in particular, the two order of a magnitude difference in abiotic oxidation  
107 rates between pyrrhotite and chalcopyrite. These rates quantitatively predict that any acid production from 'in situ'  
108 mining of SMS deposits will be buffered by advecting seawater and that mine waste has the potential to persist on  
109 the seafloor for years without complete oxidative transformation (Bilenker et al., 2016). However, these studies are  
110 typically undertaken with relatively large grain size fractions > 45  $\mu\text{m}$  and are representative of 'in situ'  
111 mining/extraction rather than the potentially more impactful dewatering and return processes that involves grains <  
112 8 $\mu\text{m}$ . Furthermore, these studies do not take into consideration any potential galvanic effects that may occur within  
113 a natural SMS ore that contains a range of co-existing sulphide minerals. A galvanic cell occurs where two  
114 different sulphide minerals are touching in the presence of an electrolyte such as seawater. The mineral with the  
115 lower resting potential behaves as an anode and preferentially dissolves, protecting the other mineral which is  
116 behaving as a cathode (Fig 1; Mehta and Murr (1983)). As highlighted by Heidel et al. (2013), pyrite in contact with  
117 most common SMS sulphide minerals should be galvanically protected as a result of a high rest potential  
118 compared to the other most common sulphides (Fig. 1). Within a seafloor context (higher pH's), this is similarly  
119 expected to be the case; where even though rest potentials are lower, the relative difference of rest potential  
120 between the minerals is constant. Galvanic cells have already been shown to increase dissolution and explain  
121 observations within the context of terrestrial sulphide ore deposits (Abraitis et al., 2004a; Heidel et al., 2013; Koski  
122 et al., 2008; Kwong et al., 2003; Li et al., 2006; Liu et al., 2008) and have also been put forward to explain  
123 observations of the mineralogy of oxidised SMS deposits (Webber et al., 2015). Whilst not attributed to galvanic

124 cells, (Edwards et al., 2003) demonstrated that a mixed sulphide ore is notably more reactive on the seafloor than  
125 individual sulphide minerals, albeit in the presence of bacteria.

126  
127 SMS deposits are comprised of a variety of mineral grains, each often containing various inclusions, and it is the  
128 galvanic interaction of these phases that may have the ability to substantially increase dissolution rates. The only  
129 leaching study that simulates natural mixed sulphide rich sediments in seawater was undertaken as a result of  
130 prospecting and a regulatory need to provide an environmental impact statement (EIS) for mining the Solwara-1  
131 Deposit, Bismark Sea, Papua New Guinea (Gwyther, 2008). There are two parts to that study, the first undertaken  
132 by Australia's Commonwealth Scientific and Industrial Research Organisation (CSIRO) (Simpson et al., 2007), the  
133 second undertaken by Charles Darwin University (Parry, 2008). Whilst extensive leaching of a range of metals is  
134 observed, the mineralogy of the ore used in experiments is not documented and only the bulk chemistry of the  
135 ores is available (as reported in Supplementary Material A).

136  
137 There is clearly a need for further studies that attempt to reproduce the true compositional range of the  
138 materials that will be dispersed into the water column as a result of deep sea mining in a colder, deeper (high  
139 pressure) more saline, and alkaline aqueous medium. This suspended particulate will include a variety of  
140 minerals; many of which will have interfaces (or inclusions) that could lead to galvanic cells. These have the ability  
141 to substantially increase the leaching of metals into the water column (Abraitis et al., 2004b; Heidele et al., 2013;  
142 Koleini et al., 2010; Kwong et al., 2003; Li et al., 2006; Liu et al., 2008; Majuste et al., 2012; Mehta and Murr, 1983;  
143 Subrahmanyam and Forssberg, 1993). There are a multitude of variables to consider in this process including  
144 mineralogy, bulk elemental chemistry, grain size distribution and surface area of the particles, pH, temperature,  
145 pressure, salinity, dissolved oxygen and prevailing ocean currents. Mineralogy and geochemistry varies  
146 considerably across sulphide ore deposits (Cherkashev et al., 2013; Hannington et al., 2005) as a result of factors  
147 including tectonic setting (influencing the composition of the host rock), pressure, pH and temperature. As a result  
148 of this, different extant ore deposits are expected to be oxidising and releasing a variety of different metals into the  
149 oceans, all at different rates.

150  
151 In this study, we begin to evaluate the potential for anthropogenic leaching of SMS ore as a result of future  
152 seafloor mining. The important questions are: Whether leaching occurs and to what extent; Are certain deposits  
153 more of an environmental risk to mine and require greater dilutions to meet toxicity guidelines; How will mineralogy

154 and geochemistry play a role in this process. To address some of these questions we have performed a series of  
155 leaching experiments that investigate some of these variables for the TAG deposit. In particular, the selected  
156 samples represent the diverse mineralogy from within this single ore deposit.

157

158 Three terms are used within this study to refer to the different processes occurring during leaching. **Leaching** is  
159 the total loss of mineral solutes by the action of a liquid (seawater). In this context, the loss of minerals (sulphides)  
160 is a result of their oxidative dissolution in seawater. The total amount of metals leached (lost) is not necessarily  
161 **dissolved** in the subsequent leachate (seawater) due to the **precipitation** of Fe oxide/oxy-hydroxides and  
162 sequestration of metals onto oxides. The term **dissolved** refers to the metals remaining in the seawater (after  
163 filtration and removal of oxides).

## 164 **2 Materials**

165 Samples from the TAG deposits, Mid-Atlantic Ridge (MAR) were supplied through the Integrated Ocean Drilling  
166 Program (IODP). Cores were recovered from five sites along the TAG hydrothermal mound (Fig. 2) during Leg 158  
167 of the IODP between October and November 1994 (Humphris et al., 1996, 1995). The five areas are named TAG-  
168 1 to TAG-5, where TAG-1 is located closest to the centre of the mound, approximately 20 metres SE of the black  
169 smoker complex. 3 TAG samples were chosen for experiments as a result of their range in mineralogy as well as  
170 availability of material. TAG samples H and J are taken from TAG-4 area, west of the central black smoker  
171 complex and TAG B is taken from TAG-3, SW of the Kremlin area (Fig. 2).

172

173 An aliquot of each TAG sample was cut, mounted in epoxy and polished as a block for characterisation of the  
174 whole rock sample. The remainder was crushed using a pestle and mortar and dry sieved to a size of <45 µm.

175

176 To ensure that any observed heavy metal leaching is a true reflection of the surface area with clean surface (as  
177 though freshly mined) and to control grain size, all fine sulphide and oxide particles (<2.5 µm) were removed. As a  
178 result of mixed sulphide ores being used in experiments and the high solubility of sphalerite and galena at low pH  
179 (Abratis et al., 2004b; Heidel et al., 2013; Malmström and Collin, 2004; Weisener et al., 2004), a cleaning method  
180 was adopted from Romano (2012). The cleaning method included 5 minutes of ultra sonication in acetone, a 5  
181 minute ethanol rinse through 2.5 µm filter paper, drying in a desiccator, agitation in 1M HCl for 30 seconds

182 followed by a 5 minute soak, with a final ethanol rinse through 2.5  $\mu\text{m}$  filter paper before drying in a vacuum  
183 desiccator.

184

185 This cleaned 2.5 - 45  $\mu\text{m}$  size fraction was always stored at room temperature in a vacuum desiccator to prevent  
186 oxidation, and individual aliquots were removed for characterisation and leaching experiments.

### 187 **3 Characterisation**

188 TAG samples were characterised as polished blocks as well as cleaned powders prior to leaching experiments.  
189 Unfortunately, it should be noted that reacted sulphide material (and any oxide phases that had formed during the  
190 experiment) was not retrieved or analysed posterior to experiments as it proved too fine to identify individual oxide  
191 particles for characterisation and too small in volume for powder X-Ray diffraction (XRD) analyses.

#### 192 **3.1 Sulphide ore Blocks**

193 Polished blocks of each sample were examined by reflected light microscopy to identify the major ore minerals and  
194 subsequent scanning electron microscopy (SEM) with an energy-dispersive X-ray (EDX) detector for further  
195 identification of phases and their semi-quantitative elemental compositions. The SEM instrument used was a Carl  
196 Zeiss Sigma<sup>TM</sup> variable pressure SEM with a Gemini<sup>TM</sup> field emission electron column with Octane-Plus<sup>TM</sup>  
197 silicon drift detector. The instrument utilises TEAM analytical software from EDAX. Table 1 provides a summary of  
198 the phases identified, their abundances (wt %), textures and the inclusions observed. Representative reflected  
199 light photographs of each sample along with SEM backscattered images are shown in Fig. 3.

200

201 In addition, some laser ablation-inductively coupled plasma-mass spectrometry (LA-ICP-MS) spot analysis (wt%  
202 ppm) were collected on some Cu-poor phases (included in Table 2). This data was collected to help provide an  
203 explanation of dissolution results as well as an indication of which minerals are likely to be dissolving. LA-ICP-MS  
204 analyses were carried out using a Nu Instruments ATTOM HR-ICP-MS at GEOMAR, Helmholtz Centre for Ocean  
205 Research, Kiel. For detailed methodology, please refer to Supplementary Material B.

#### 206 **3.2 Sulphide ore powder**

207 Powder XRD was conducted using a Phillips X'Pert Pro diffractometer with a Cu  $K\alpha$  source, detailed methodology  
208 is outlined in Supplementary Material C. This provided an overall representation of the phases present including



209 semi-quantitative analysis presented in Table 1 with individual XRD patterns shown in Supplementary Material C1.  
210 An aliquot of each cleaned sulphide powder was mounted in resin and polished to 1  $\mu\text{m}$  diamond grade. This  
211 allowed for identification of mineralogy of individual grains and inclusions (Fig. 4). Bulk Fe and Cu data of all  
212 powder samples are also presented in Table 1. Samples underwent aqua regia digestion, with arising solutions  
213 analysed on an SPECTRO Ciros SOP inductively coupled plasma - optical emission spectrometer (ICP-OES) at  
214 the University of Kiel, Germany. For a more detailed methodology, please refer to Supplementary Material D. As  
215 there is the potential for a wide distribution of grain sizes in between the resulting 2.5 – 45  $\mu\text{m}$  size fraction of  
216 sulphide powders, surface area analysis was undertaken to highlight any differences between samples (due to  
217 grain size and/or mineralogy) and allows for normalisation of results. The surface area of all cleaned size fractions  
218 were determined using the Brunauer, Emmett and Teller (BET) multiple point  $\text{N}_2$  surface area method, on a  
219 Quantachrome NOVA 1200 and are quoted in Table 1.

## 220 **4 Experimental Methods**

221 Seawater solutions were made according to the recipe of Millero (2013). They were found to contain on average  
222  $391.96 \pm 27.66$  ppb Fe,  $172.63 \pm 39.16$  ppb Cu and  $73.85 \pm 19.41$  ppb Pb as contaminants. Approximately 0.6 - 1 g  
223 (dependent on availability) of natural TAG sulphide ore of 2.5 - 45  $\mu\text{m}$  was added to 500 mL of seawater.  
224 Conductivity, pH and dissolved oxygen (DO) readings were taken throughout the experiments using a HACH  
225 meter. Conductivity was calibrated at 12.85 and 53.0  $\text{mS cm}^{-1}$  and pH measurement was calibrated at 4.01 and 9.  
226 All experiments were stirred using a magnetic flea, the rate of stirring was chosen so that particles remained  
227 suspended, analogous to a dewatering of the ship-board ore in a mining context. Temperatures were held at  
228 approximately  $12 \pm 1$   $^\circ\text{C}$  (simulating the sea surface) using a refrigeration unit. Dissolved oxygen concentrations  
229 were controlled by varying the ratio of compressed air to nitrogen using sintered flow meters and were held at  
230 approximately  $9.0 \text{ mg L}^{-1}$  across the duration of each experiment. This oxygen concentration is representative of  
231 concentrations within proximity of the TAG hydrothermal field, where values in the Atlantic (A05) eWoce database,  
232 show a range between 8.2 and 8.856  $\text{mg L}^{-1}$  with the highest concentration observed at 5 km depth at a  
233 temperature of 1.5  $^\circ\text{C}$  (Schlitzer, 2000). Features of individual experimental runs are summarised in Table 3.  
234  
235 During each experimental run, trace amounts of sulphide material were lost onto the surfaces of monitoring probes  
236 and during sample filtration. In order to account for this, the wastewater was filtered, desiccated and weighed, and  
237 the value subtracted from the initial weight, as shown in Table 3.

## 238 4.1 Sampling protocol

239 Dissolution experiments adopted a semi-batch design, as described in Rimstidt and Newcomb (1993) and Salmon  
240 and Malmström (2006). Seawater samples (13 mL for metal analysis) were removed using a 10 mL mechanical  
241 pipette (with an error of 0.5%) for analyses. 13 mL of fresh seawater is added to replace the volume lost at each  
242 sampling interval (total of 156 mL over the course of each experiment), with any resultant dilution corrected for  
243 (see Section 4.3).

244

245 Removed batch samples were filtered using a 0.22 µm pore size to remove all sulphide material and halt any  
246 further reaction. Sampling occurred every 10 minutes for the first hour, every half an hour for the following two  
247 hours and every hour up to the full 5 hours run time. 5 hours run time was chosen to be representative of the  
248 amount of time it would take for a steady state to occur between the sulphide and seawater and also reflects the  
249 period of agitation related to SMS mining.

250

251 Extracted aliquots were analysed using an Agilent 710 ICP-OES. Filtered (0.22 µm) solutions were acidified with  
252 2% HNO<sub>3</sub> in a 2:1 ratio (3 mL sample to 6 mL of nitric acid) to prevent metals from precipitating out and to lower  
253 the total dissolved solids to <1%. All samples were analysed for Fe (234.350), Cu (327.395), and Pb (220.353)  
254 with chosen emission lines in brackets. Units of measurement are µg/L, referred to here as ppb. Standards for  
255 metals ranged from 1-10 ppm. Limits of detection for the ICP-OES for Fe, Cu, and Pb are 0.70, 1.22, and 6.52 ppb  
256 respectively.

## 257 4.2 Corrections

258 To account for 13 mL of sample removal and subsequent dilution with 13 mL of fresh seawater, the equations of  
259 Salmon and Malmström (2006) were used (Eq. 5). This calculation assumes that elements measured in previous  
260 samples remain in solution. The accumulated amount,  $N$ , of element  $j$  remaining in solution up to sample  $k$ ,  
261 calculated from the measured concentration,  $C_{meas}$ , is determined by:

262

### 263 Equation 5

$$264 N_{k,j} = \left[ C_{k,j,meas} (V_{0,total} - V_{k,ret}) + \sum_{s=1}^k C_{k,j,meas} V_{s,sample} \right]$$

265

266 All analysed solutions were also corrected for the dilution with nitric acid and initial seawater composition (including  
267 removing seawater starting concentrations of Fe, Cu and Pb). These 'corrected' concentrations will henceforth be  
268 referred to as 'measured' concentrations.

269

270 Measured concentrations were subsequently combined with other data (mass, surface area) in order to highlight  
271 the implications for SMS mining. To identify the effect that bulk chemistry and different mineral mixtures (and  
272 galvanic effects) exerted on leaching and metals observed in solution, absolute measured concentrations (ppb)  
273 require a correction for the variability of sample mass used in each experiment. This correction is outlined in Eq. 1  
274 in Supplementary Material E. To assess the potential metal leaching during mining scenarios, absolute measured  
275 concentrations (ppb) require a series of corrections including 1) conversion to  $\mu\text{mol}$  2) correction for volume of  
276 seawater used and 3) a correction for the sample mass and surface area. These correction procedures are  
277 outlined in Eq. 2 and Eq. 3 in Supplementary Material E. In this way, results can be extrapolated for leaching  
278 outside of the fixed rock to fluid ratio (g/L) using here.

## 279 **5 Results**

280 Actual measured concentrations and errors (ppb), without corrections for surface area, mass of ore and volume of  
281 seawater are presented in Supplementary Material F1. However to compare between different samples it is more  
282 informative to correct these values to reflect the mass (g) of ore used (Section 5.1) as well as the different  
283 available reactive surface areas (Section 5.1)

### 284 **5.1 Concentrations corrected for mass, volume and surface area ( $\mu\text{mol}/\text{m}^2$ )**

285 Measured concentrations and errors (ppb) converted to  $\mu\text{mol}$  and corrected for surface area, volume of seawater  
286 and mass of ore used are presented in Figure 5, using data produced in Supplementary Material F2. Shown for  
287 reference are representative maximum solubility's of Cu, Fe and Pb in seawater taken from experimental and  
288 calculation studies (Angel et al., 2015; Franklin et al., 2001; Liu and Millero, 2002). As noted in Figure 5 and  
289 discussed in Section 6, all elements (but particular Fe) may show an increase in the seawater as the metal is  
290 leached and/or a decrease as the metal is removed from solution by precipitation of or absorption onto an oxide.

### 291 5.1.1 Cu

292 All samples show an initial rapid leach of Cu producing a concentration peak measured at the beginning of each  
293 experiment but differing in magnitude and time between samples. The maximum concentration peaks for Cu are  
294 up to:  $3.89 \pm 0.07$ ,  $0.47 \pm 0.26$  and  $2.37 \pm 0.09$   $\mu\text{mol}/\text{m}^2$  for TAG-B, H, and J respectively. This initial leach then drops  
295 significantly and remains at a more consistent level. After 30 minutes, the average dissolved Cu was  $0.09 \pm 0.018$ , -  
296  $0.04 \pm 0.33$  and  $2.41 \pm 0.06$   $\mu\text{mol}/\text{m}^2$  for TAG-B, H and J. Whilst these are average values, the experiment with TAG-  
297 B shows a subsequent slow decrease in aqueous Cu down to  $0.01 \pm 0.01$  ( $\sim 0$  within error). This is in contrast to the  
298 experiment with TAG-H where there is overall negligible change in Cu, with only spikes of  $0.27 \pm 0.28$  and  
299  $0.41 \pm 0.37$   $\mu\text{mol}/\text{m}^2$  that are within error of 0 and  $0.04$   $\mu\text{mol}/\text{m}^2$  respectively. TAG-J is the only experiment where  
300 there is an initial leaching of Cu that does not decrease to 0 throughout the 300-minute sampling window. Within  
301 this average of  $2.37 \pm 0.06$ , there is a peak of  $2.69 \pm 0.06$   $\mu\text{mol}/\text{m}^2$ . From the 90 minute sampling interval onwards,  
302 the amount of Cu dissolved decreases from this peak value but only down to  $2.04 \pm 0.06$   $\mu\text{mol}/\text{m}^2$ .

### 303 5.1.2 Fe

304 All samples show an initial leach of Fe to the seawater producing a peak at the beginning of each experiment similar  
305 to the observed behaviour of Cu, except here Fe concentrations exceed the solubility limit of seawater. Again,  
306 similar to the Cu peak, the magnitude of the Fe peak differs between samples. The initial peaks of Fe are  
307  $1.63 \pm 0.04$ ,  $0.47 \pm 0.19$  and  $0.54 \pm 0.12$   $\mu\text{mol}/\text{m}^2$  for TAG-B, H and J respectively. This initial dissolved concentration  
308 then drops to negative Fe values after the 20-minute sampling interval for experiments with TAG-B and TAG-H  
309 and after the 90-minute sampling interval with TAG-J. At the 120-minute sampling interval, TAG-H displays a spike  
310 in Fe concentration at  $0.99 \pm 0.19$   $\mu\text{mol}/\text{m}^2$  which does not correspond to either of the Cu spikes of the same  
311 experiment. The fall to negative values (below initial seawater background) is consistent with the precipitation of Fe  
312 oxides and exceedance of the solubility limit of Fe in seawater.

### 313 5.1.3 Pb

314 Whilst there is an initial leaching of Pb in experiments with TAG-H and TAG-J, in contrast to the behaviour of Cu  
315 and Fe in the same experiments, the initial dissolved Pb is comparable to later sampling intervals. The initial peaks  
316 of Pb are  $0.18 \pm 0.16$  and  $0.20 \pm 0.13$   $\mu\text{mol}/\text{m}^2$  for TAG-H and J respectively. TAG-B shows negligible leaching  
317 initially and throughout the experiment with the exception of small spikes at the 20 and 90-minute sampling  
318 interval, which are within error of 0.

319

320 TAG-H and TAG-J show consistent net dissolved Pb throughout the entirety of the experiments. Whilst there are  
321 fluctuations during each experiment, there is no overall increase or decrease in the dissolved concentrations of Pb.  
322 Across the whole experiment there is an average dissolved concentration of  $0.17 \pm 0.16 \mu\text{mol}/\text{m}^2$  and  $0.16 \pm 0.11$   
323  $\mu\text{mol}/\text{m}^2$  of Pb for TAG-H and TAG-J respectively. However, the maximum Pb dissolved throughout the 300  
324 minute-sampling interval is  $0.38 \pm 0.12 \mu\text{mol}/\text{m}^2$  versus  $0.27 \pm 0.08 \mu\text{mol}/\text{m}^2$  for TAG-H and TAG-J respectively.

## 325 **5.2 Concentrations corrected for mass (ppb / g)**

326 Results presented in  $\mu\text{mol}/\text{m}^2$  cannot be used to directly infer the effects of mineral mixtures, as the surface area of  
327 the ore used within the correction for each sample is a summation of the surface area of multiple different mineral  
328 phases. Instead, measured concentrations and errors (ppb) corrected for grams of ore used in each experiment  
329 are presented in Figure 6. Data are presented in Supplementary Material F3. Furthermore, data presented in this  
330 way can provide an idea of the actual magnitude of dissolved metals when scaled up to ore production quantities.

331

332 TAG-J shows the highest dissolved concentration of metals in seawater, on average (from the 30 minute sampling  
333 interval)  $186.01 \pm 4.96$  ppb Cu per gram of ore and  $39.45 \pm 26.54$  ppb Pb per gram of ore. TAG-H shows similar  
334 concentrations of Pb to TAG-J, with an average of  $42.78 \pm 37.74$  ppb per gram of ore after the 30-minute sampling  
335 interval.

## 336 **6 Discussion**

337 Seafloor SMS material that is disturbed during in situ mining, along with fine particulate SMS materials returned to  
338 the ocean after surface processing will initially be suspended in the water column as a sediment plume and may  
339 be dispersed into the wider ocean, but will ultimately settle out onto the seafloor. Whilst there is still the potential  
340 for toxicity and leaching, the in situ extraction is argued to pose less of a risk as a result of the larger grain sizes of  
341 the arising particulates (less surface area available for leaching as well as a quicker settling rate, reducing the time  
342 the sulphide is exposed for leaching) (Gwyther, 2008). In particular, a study by Bilenker et al. (2016) suggests that  
343 acid generation during in situ mining is slow and unlikely to be problematic.

344

345 Leaching experiments presented in this study are most representative of the dewatering process during ship-board  
346 processing and return of material to the sea, where finer particles are exposed to seawater. During exposure there

347 is potential for these fine sulphide particles to experience more substantial dissolution and release of heavy  
348 metals, both locally or some distance into the open sea. Quantification of the distal extent of such plumes and  
349 subsequent leaching is difficult to speculate upon without modelling of site-specific plume generation. To this end,  
350 stochastic hydrodynamic modelling from Gilbert et al. (2008) was used to investigate the impact of discharging  
351 return water at Solwara 1, and the results are applicable to experiments here. The modelling involved a range of  
352 variables (dilution rates, temperatures) and found that plumes would dissipate and achieve a dilution of 5000 times  
353 within 0.6 km from the point of discharge. The estimated maximum sub-sea plume thickness within the water  
354 column is 175 m.

355

356 Whilst the Gilbert et al. (2008) model demonstrates that the concentration of fine material ( $<8 \mu\text{m}$ ) dilutes fairly  
357 rapidly with distal extent, the time it will take for it to fall to the seafloor (and out of the water column) from the  
358 designated 25 to 50 m height above the seafloor is not stated. During this time, it will be exposed to seawater,  
359 allowing leaching to progress. Experiments in this study demonstrate the early dissolution of metals, with high-  
360 resolution time steps. Gilbert et al. (2008) state that over the lifetime of the mining operation (20 months), the peak  
361 bottom thickness from the settling fine material is less than 0.1 mm. Based on assumptions made in the modelling  
362 as applied to the EIS and using Stokes Law, an  $8 \mu\text{m}$  pyrite particle (density of  $5 \text{ g/cm}^3$ ) would take 1.87 days to  
363 settle out from a height of 50 m. However, a  $0.1 \mu\text{m}$  pyrite particle, would take 12010 days to settle from a 50 m  
364 height above the seafloor. Without a better understanding of the grain size distribution within the  $<8 \mu\text{m}$  size  
365 bracket, it is difficult to quantify the amount of time sulphide material will ultimately persist and leach in the water  
366 column. Furthermore, even after any fine material has settled, whilst the surface area exposed has been reduced,  
367 there is still potential for further leaching of metals as the material lies as a poorly consolidated seafloor deposit.

368

369 The experiments of this study simulate the consistent stirring of sediments and as a result, the ore has the  
370 maximum exposure for leaching. This is representative of the early leaching process that will occur prior to settling  
371 or dilution, especially in the finer fraction.

372

373 Within the first 10 minutes, all samples show initial dissolved concentrations of Cu and Fe, at varying magnitudes  
374 (Fig. 5). Fig. 7 demonstrates the average dissolved metal as a proportion of the bulk concentration, expressed as a  
375 percentage. Whilst percentage dissolved values are in themselves small, it is important to note the high bulk  
376 concentrations of heavy metals in the TAG samples; making this small loss significant in terms of toxicity. TAG-H

377 demonstrates the highest initial percentage loss of Cu and Pb, whilst TAG-B shows a high loss of Cu and TAG-J a  
378 loss of Pb.

379

380 Using the data of this study as a 'realistic' example (although this ignores any abiotic contribution), these results  
381 suggest that a total of 0.04 and 0.002 wt% of Cu, Fe and Pb will be leached from a deposit such as TAG-H and  
382 TAG-B respectively, at the initial stages of processing (Fig. 7). However, with removal of both Cu and Fe from  
383 solution by oxide precipitation after 10 minutes (based on exceedance of solubility limit and observation), this  
384 effect is reduced even more dilution subsequently occurs.

385

386 A deposit such as TAG-J is more concerning. 0.03 wt% of Cu, Fe and Pb will be lost in the initial stages of  
387 processing (Fig. 7a), but leaching of Cu and Pb will continue (Fig. 7b) until either the particle interface has been  
388 fully dissolved or an oxide forms on the particle surface and insulates it from the seawater (passivation on the  
389 surface, which is expected in most cases). However, the fact that precipitation of oxides is not shown to remove  
390 the dissolved metals for TAG-J is a cause for concern. In the TAG experiments where a loss is observed, Pb and  
391 Cu have the highest percentage dissolved, indicating their higher propensity to be leached and stay in solution  
392 compared to Fe. This is also observed in experiments undertaken in the EIS (see Fig. 7).

393

394 Sample TAG-J shows the only sustained dissolved concentrations of all the experiments in this study, with both  
395 Cu and Pb present in seawater, remaining at a significant level (Fig. 5, 6 and 7). Whilst all three TAG samples  
396 contain similar concentrations of Pb (100-200 ppm, Table 1), it is only TAG-H and TAG-J that show leaching of Pb  
397 into seawater (both at ~ 40 ppb). TAG-B, a sample that contains a similar, if not higher, total amount of  
398 chalcopyrite and bulk Cu as TAG-J (Table 1), shows initial leaching of Cu (Fig. 5), but this is removed after 30  
399 minutes.

400

401 Due to the design of these experiments, precipitations of metal oxides are guaranteed under these high pH  
402 conditions in all experiments, mainly precipitating Fe-oxide, but also having the potential to sequester and remove  
403 Cu and Pb. All were run at similar oxygen concentrations where oxygen was never limited and kept constant  
404 throughout, ensuring the formation of oxide precipitates throughout the course of experiments, (Table 3), yet both  
405 TAG-J and TAG-H have sustained dissolved metals that are not removed from solution. This indicates that the  
406 leaching of Cu from TAG-J is at a higher magnitude than any removal through oxidation (due to mineralogy or

407 galvanic effects) and that the method of removal of Cu and Pb from TAG-B is different to TAG-J and TAG-H (due  
408 to mineralogy). This is discussed further in Section 6.1. Either way, the leaching results demonstrate that bulk  
409 chemistry does not dictate the concentration of metals dissolved into seawater. Instead, mineralogy and/or  
410 possible galvanic effects are the driving forces behind the type and concentration of metals remaining in seawater  
411 after leaching.

412

413 As shown in Fig. 6a, b and c, the high concentrations of Fe and Cu dissolved in experiment TAG-J are very similar  
414 to those observed in experiments from the EIS. The figure shows results from two different published experimental  
415 datasets that have the most similar run conditions to those used in the current study. The specific mineralogy of  
416 the samples used within the EIS was not presented for either the experiments of Parry (2008) or Simpson et al.  
417 (2007), although the overall chemistry was provided and is reproduced in Supplementary Material A. Based on this  
418 chemistry, the mineralogy is substantially different between each of their experiments.

419

420 Data from Parry (2008) uses predominantly Fe-rich samples (31.6 % Fe, 5.13 % Cu, 3670 ppm Zn) similar to our  
421 experiments with deposits from TAG (Table 1, bulk Fe and Cu) with Cu and Pb dissolved at similar concentrations  
422 as TAG-J, despite a larger grain size, and higher temperature and rock-fluid ratio. Studies by Moses and Herman  
423 (1991) and Simpson et al. (2007) indicate a linear relationship between rock to fluid ratio and dissolved metals,  
424 allowing for data to be scaled to take into consideration the difference in rock-fluid ratio between studies. When  
425 data from Parry (2008) is scaled to the rock-fluid ratio used in this study (2 g/L), concentrations drop to ~3 ppb for  
426 Cu and ~2 ppb for Pb. This lower concentration/lower percentage loss of bulk observed in the EIS data when  
427 scaled to 2 g/L (Fig. 6 & 7) can be explained by the larger grain size (less surface area) used in experiments.

428

429 The ore used in experiments by Simpson et al. (2007) has significantly higher bulk Cu, Zn, Pb and As than ore  
430 used by Parry (2008) and the TAG samples used here (Supplementary Material A). Despite this, the dissolved Cu  
431 and Pb is much lower than the comparable experiments with Fe-rich ore as shown in Fig. 7. This is comparable to  
432 our results, where bulk chemistry does not define the metals that are leached and remain in solution. What is not  
433 shown in this figure, is the high dissolved concentrations of Zn and As during the EIS experiment with the Cu-Zn-  
434 Pb rich ore (Supplementary Material A). This could imply a preferential dissolution of Zn and As rich minerals (e.g.  
435 sphalerite and arsenopyrite/As sulfosalts) over Cu and Fe, suggesting either galvanic cells are at play or that the  
436 dissolution rate of Zn and As bearing minerals is quicker.



437

438 Based on the effect differing mineralogy has on the leaching of SMS ores presented in this study, it is imperative  
439 that extensive tests with the full range of mineralogy and geochemistry of ore mined are undertaken prior to any  
440 future mining of a deposit. Results where only one type of ore are utilised in experiments are applicable to only a  
441 particular area of a deposit and are not ubiquitously transferable.

## 442 **6.1 The effect of mineralogy on leaching and dissolved metals**

443 By combining the observed mineral proportions and bulk chemistry from Table 1 with the magnitude of metal  
444 released to the seawater (ppb), corrected for grams of ore tested (Fig. 6), it should be possible to at least  
445 speculate on the effect that mineralogy, texture and possible galvanic reactions might have on the 'leaching'  
446 process. It must be remembered that the 'leaching' simulated here and in particular the monitoring of metal release  
447 with time as sulphide dissolves, will be counteracted by subsequent oxide precipitation in these experiments. The  
448 measured metals in solution can only give a net view of the two competing processes. The dissolved oxygen levels  
449 in the seawater have been fixed at a value that is representative of the TAG field in these experiments (Schlitzer,  
450 2000) although this could be a local variable. Fe is the major contributor to the precipitate (due to its low solubility  
451 in seawater), forming Fe oxides/oxy-hydroxides. The 'absorption' of other heavy metals (e.g. Cu, Pb) onto Fe  
452 oxides and oxy-hydroxides has been extensively demonstrated in the literature (Benjamin and Leckie, 1981;  
453 Davranche and Bollinger, 2000; Grybos et al., 2007; Jong and Parry, 2004; Liu and Huang, 2003). Absorption of  
454 trace metals onto (and subsequently into) iron oxides and oxy-hydroxides is observed to be rapid, on the time  
455 scale of hours, (Ahmad et al., 2012; Balistrieri and Murray, 1982) so it likely to be an important process on the  
456 timescale of this study as well as the actual mining operation. It is unfortunate that design of the current study  
457 produces too small an amount of precipitate to collect and measure the trace metal composition.

458

459 In addition to the new Fe-oxide precipitation, some ore samples such as TAG-B initially contain a high proportion  
460 of Fe oxides and oxy-hydroxides (Fig. 3, Table 1) that would represent a large surface area of the processed ore  
461 material, and will be present at the beginning of our leaching experiments. This could represent either a source to  
462 release metals or remove them in a similar way to the newly formed Fe precipitate. In the latter case, the presence  
463 of Fe oxides/oxy-hydroxides within the deposit prior to mining (likely in the case of an inactive SMS deposit) could  
464 be advantageous in reducing the environmental toxicity associated with mining.

465

466 Samples have all been crushed and sieved to the same grain size fraction (2.5 to 45  $\mu\text{m}$ ) to remove this as a  
467 variable between experiments. Whilst there is the potential a range of distributions within this size fraction, this  
468 potential should be eliminated during the normalisation of the data to the surface area of each specific sample (Fig.  
469 5).

470

471 All samples here show an initial increase in Fe, which is undoubtedly caused by sulphide ore dissolution. This is  
472 followed by a rapid decrease to background levels in a few hours, although TAG-B and H fall more rapidly than  
473 TAG-J. The solutions are observed to fall below the original background seawater levels (Fig. 5 and 6), indicating  
474 that in some cases the original seawater Fe is removed from solution (oxidised) also. The dissolved oxygen  
475 concentration is kept constant throughout the experiment, ensuring they are never oxygen limited and it is possible  
476 to continuously form oxides as would be expected in the natural environment. The fall in Fe is either due to a one  
477 off initial release and subsequent precipitation of Fe as an oxide with time, or an increase in the precipitation rate  
478 over the continuous release rate.

479

480 All three TAG samples contain similar Pb concentrations (100-200 ppm), yet only samples TAG-H and J show  
481 leaching. No galena or major Pb bearing minerals were identified in the samples, indicating that the Pb must arise  
482 from the lattice sites of sulphide phases (Table 2), though it is not possible to identify the particular mineral phase  
483 contributing the Pb from this data alone. The observation that TAG-B has negligible Pb dissolved whilst  
484 demonstrating similar bulk Pb suggests that Pb is present as a phase that is not leaching or more stable (e.g.  
485 sorbed onto present Fe oxy-hydroxide).

486

487 Based on bulk analysis alone (Table 1), it might be expected that TAG-B would demonstrate the highest Cu  
488 release and concentration in the seawater. Whilst it does leach the highest initial concentration of Cu (Fig. 5), it is  
489 TAG-J that maintains the higher dissolved Cu throughout the 300-minute experiment. It is clear from the TAG-J  
490 experiment that the formation of oxides does not keep up with the leaching of Cu, resulting in consistently high  
491 dissolved Cu. The disparity between TAG-B and J can ultimately be explained by either 1) a different Cu  
492 host/source, 2) a difference in mechanism leaching Cu, 3) a difference in mechanism removing Cu or 4) a  
493 difference in exhaustion/isolation (passivation) of Cu host/source. These possibilities are discussed in further detail  
494 below.

495 6.1.1 *Hosts and sources of Cu*

496 Chalcopyrite is the largest source of Cu observed in both TAG-B and TAG-J (6.2 and 5.6 wt% respectively). In  
497 reality, chalcopyrite has been shown to have at least an order of a magnitude slower dissolution rate than both  
498 pyrite and marcasite (Bilenker, 2011; Feely et al., 1987; Romano, 2012). As a consequence of this, a sample such  
499 as TAG-H (~42% marcasite) or TAG-J (83.8% pyrite) might be expected to dissolve the fastest and not only leach  
500 the most Fe, but also a certain amount of Cu, which is present at trace levels in the mineral lattice (see Table 2).  
501 This then could become a more important source of Cu than the major host chalcopyrite. On closer inspection,  
502 marcasite can be ruled out on the basis of two pieces of evidence: 1) low concentrations of Cu in its lattice (77.20  
503 ppm, Table 2) and 2) TAG-H has a dominant marcasite mineralogy (~42%) with similar concentrations of Cu in its  
504 lattice to TAG-J (70.75 ppm) but shows no significant release of Cu (Fig. 5).

505  
506 The role of pyrite can also be assessed. As shown in Table 2, the TAG-J pyrite contains higher concentrations of  
507 Cu in its lattice (715.30 ppm) than the pyrite in TAG-B (461.20 ppm). As TAG-J also contains 1.5 times more pyrite  
508 than TAG-B, it might appear to be a plausible source of Cu during the leaching of TAG-J. However, with high  
509 concentrations of pyrite (24.4 wt%) and high Cu in its lattice, it would be expected that TAG-B would also display  
510 consistent dissolved concentrations of Cu if pyrite breakdown were the main Cu release mechanism and  
511 proceeded at the same rate in both samples. Furthermore, if pyrite were the source in both, it would be expected  
512 that TAG-J would have an initial higher leach than TAG-B, which is not observed. Based on these observations, it  
513 is difficult to appeal to pyrite (or marcasite) as the source of released Cu.

514  
515 Another plausible Cu source to consider and explain the disparity between TAG-J and TAG-B, would be secondary  
516 formed Cu minerals. They have been demonstrated to have higher dissolution rates than chalcopyrite, but how this  
517 rate compares to pyrite and marcasite is unknown (Fullston et al., 1999). TAG-J was shown to contain rare  
518 covellite (CuS) during reflected light microscopy and XRD analysis at ~1.4 wt%. The leaching of covellite could  
519 provide a tenuous explanation for the heightened dissolved Cu in TAG-J over TAG-B, but still does not explain the  
520 higher initial leach of Cu during the TAG-B experiment.

521  
522 The observation of dissolved Cu decreasing throughout the experiment with TAG-B could suggest exhaustion of a  
523 Cu source or its isolation from the seawater. However, it would be difficult to explain why any reduction in  
524 availability is occurring throughout the experiment in TAG-B and not TAG-J based on the constant dissolved  
525 oxygen concentrations. For example, if passivation on the surface of Cu sulphide minerals (due to the formation of

526 oxides) were to occur and reduce the availability of Cu, it would be expected in both TAG-B and TAG-J  
527 experiments. Another phenomenon with the potential to explain the disparity in dissolved Cu over time between  
528 TAG-J and TAG-B is absorption, discussed earlier.  
529  
530 TAG-B contains a high quantity of Fe-oxides and oxy-hydroxides (Fig. 3) that would be present during leaching.  
531 Absorption of heavy metals onto Fe oxides and oxy-hydroxides could account for the subsequent drop in Cu over  
532 time observed during the experiment with TAG-B (Fig. 5). New oxide phases that form throughout the TAG-J  
533 experiment are unlikely to provide as high of a surface area for absorption as the already established oxides  
534 present in TAG-B do. If this is the case, the presence of Fe oxides/oxy-hydroxides within the deposit prior to  
535 mining (likely in the case of an inactive SMS deposit) could be advantageous in reducing the environmental impact  
536 associated with mining.

#### 537 6.1.2 Galvanic cells

538 Notwithstanding the presence of covellite or the process of absorption, dissolution rates of the major sulphide  
539 minerals alone cannot explain the observations found in this study. In terms of alternative causal effects, galvanic  
540 cells have been shown to significantly increase dissolution (Abraitis et al., 2004a; Heidel et al., 2013; Koski et al.,  
541 2008; Kwong et al., 2003; Li et al., 2006; Liu et al., 2008).

542  
543 Whilst it is unlikely that any separate grains would be able to stay in contact for long enough to create a cell in  
544 these stirred experiments, individual particles composed of multiple sulphide phases can create a cell with  
545 seawater. Both TAG-B and TAG-J commonly demonstrate the occurrence of sulphide inclusions in whole rock  
546 samples and cleaned sulphide ore powders (some less than 1  $\mu\text{m}$ ) of chalcopyrite in pyrite/marcasite grains and  
547 vice versa (see Fig. 3 and 4), allowing galvanic cells the ability to form during leaching experiments. In this  
548 scenario, the lower potential of chalcopyrite (Fig. 1) would cause it to be preferentially dissolved relative to pyrite  
549 (or marcasite), releasing Cu and some Fe into solution.

550  
551 TAG-B has much less pyrite than TAG-J (24.4% vs. 84% pyrite plus 6% marcasite), and consequently, fewer  
552 inclusions to allow for galvanic cells to occur. If galvanic cells were playing a role, it would be expected that both  
553 TAG-B and TAG-J would display a leach of Cu, just at a higher magnitude in TAG-J, which is not observed in the  
554 initial leach (TAG-B has a higher initial leach). However, this could be easily explained by an initial leach of

555 chalcopyrite in both that slows with time (producing the higher initial leach of Cu in TAG-B), with galvanic cells in  
556 TAG-J producing the higher dissolved Cu concentrations observed later on.

557

558 Exact quantification of the extent to which galvanic coupling, and mineralogy (and any associated absorption) is  
559 contributing to dissolution role is not possible within the scope of this study, simply because there are numerous  
560 inseparable variables at play. Nonetheless their impact on the leaching of SMS ore needs to be considered and  
561 accounted for in environmental impact predictions.

## 562 **6.2 Toxicity potential**

563 The toxicity induced by sulphide dissolution may have some detrimental impact on the environment around SMS  
564 deposits and associated ecosystems, although this will ultimately be highly variable. It has been speculated that  
565 any high concentrations of heavy metals that are leached or present in the plume will pose minimal risk to a faunal  
566 system already adapted to active SMS deposits (Simpson et al., 2007; Gwyther, 2008; Parry, 2008; Sander and  
567 Koschinsky, 2011). However the most distal 'background' fauna may not have developed such survival strategies.  
568 Furthermore, if mining occurs at inactive SMS deposits where adaptation to toxicity is lower, the impact to this  
569 specific ecosystem may be more significant; unless these ecosystems have a high recovery rate.

570

571 Initial high metal concentrations (within 10 minutes) are unlikely to cause serious problem for fauna as they are  
572 quickly removed via precipitation of oxides, with suffocation from plumes a more serious concern in the initial  
573 stages. Whilst the average percentage loss (Fig. 7) is very small across all metals and samples (<0.1%), the  
574 sustained dissolved metals at a ppb level is still considered significant due to their exceedance of both Australian  
575 and New Zealand water quality (ANZECC) and UK Marine Special Areas of Conservation (SAC) environmental  
576 guidelines. It is difficult to apply these guidelines to black smoker environments, where background toxicant  
577 concentrations vary significantly and the ecosystems are dramatically different to 'normal' marine ecosystems. In  
578 fact, no guidelines exist for such environments. For purposes of discussion and to compare experiments  
579 undertaken here with those undertaken in the EIS by Solwara-1, the minimum guideline for each metal has been  
580 chosen (99% protection, ANZECC). Guidelines are 0.3 and 2.2 ppb for Cu and Pb respectively.

581

582 Based on the current mining concept outlined by Nautilus Minerals for their EIS, the return water will include solid  
583 material <8 µm in diameter with an expected total dissolved solids (TDS) of 6.35 g/L (Gwyther, 2008) compared to

584 the 2 g/L of this study. When experiments in this study are scaled to the rock-fluid ratio outlined in the EIS  
585 (Supplementary Material G), Cu concentrations observations in TAG-J would increase to an average of  $590.6 \pm 15.7$   
586 and Pb to  $133.4 \pm 84.8$  ppb. TAG-H's Pb concentrations would increase to an average of  $135.8 \pm 119.8$  ppb. These  
587 are well above guidelines before dilution is taken into consideration.

588  
589 Based on experiments with 2 g/L, TAG-J would require 620 times dilution to reduce Cu concentrations to within the  
590 0.3 ppb ANZECC guideline. When scaled to the expected 6.35 g/L rock to fluid ratio, a 1968 times dilution would  
591 be required during mining. For TAG-H at 2g/L, a 19.4 times dilution would be required to bring the Pb  
592 concentration in line with the 2.2 ppb UK-SAC guideline. This would increase to 61.7 times if scaling the  
593 concentrations to the 6.35 g/L ratio. Elutriate experiments undertaken by Simpson et al. (2007) find that dilutions of  
594 greater than 4000 times may be necessary for samples from Solwara, double the values suggested by this study.  
595 The higher dilution requirement is likely to accommodate the high observed concentrations of As and Zn in their  
596 dataset, elements which were not considered in this study. Whilst it is likely that As and Zn are present in higher  
597 concentrations at Solwara than the TAG samples used here, data from Solwara experiments and trace element  
598 studies (e.g. Hannington et al. (1991) and Wohlgemuth-Ueberwasser et al. (2015)) suggest that As, Zn, Co and Cd  
599 could be leached during mining, and thus will require further investigation.

600  
601 If the 2 g/L rock to fluid ratio is kept constant, localised toxicity would be expected in a stagnant water column.  
602 However, in reality, dilution is expected where both plumes created by dewatering or extraction and deep-sea  
603 currents have the ability to entrain fresh seawater. Hydrodynamic modelling can give an indication of dilution of  
604 heavy metal concentration with distance but is site specific and does not take into consideration the time it would  
605 take for dilution to occur. Gilbert et al. (2008) demonstrate a 600-fold volume dilution would be achieved within 85  
606 m of the point of discharge at Solwara-1. However if TAG dissolved metal concentrations of this study were scaled  
607 to 6.35 g/L, a 2000 fold volume dilution is required which would only be achieved at 600 m from the discharge.  
608 Ultimately, the distance at which dilution is achieved to meet guidelines may not be sufficient, indicating either the  
609 potential need for ship-board dilution prior to the return of waste water or refinement of the mining process. Of  
610 more concern is that this does not include any ore particulate remaining in the diluted seawater volume, which may  
611 continue to release further metals to solution during any dilution process.

612

613 In terms of total input into the ecosystem, the EIS for the proposed Solwara-1 deposit in Papua New Guinea  
614 currently suggests a footprint of approximately 0.112 km<sup>2</sup> will be mined over five mineralised areas. If an area of  
615 that size at TAG was to be mined and was identical in mineralogy, bulk chemistry and texture to TAG-J, there  
616 would be a cumulative total of 0.224 moles of Cu (14230 ppm) added to the seawater throughout the mining  
617 project.

618  
619 Application of the data from this study and the Solwara-1 EIS might be 'conservative' if a finer ore size fraction (<8  
620 µm) is taken into consideration. This could result in a significantly higher surface area and higher leaching rate.  
621 The potential for toxicity during dewatering would be far more substantial than observed during the course of these  
622 experiments. In addition, there are SMS deposits that are known to contain considerably higher concentrations of  
623 toxic metals (As, Pb, Sb, Zn, Co, Cd, Ni and Hg) than TAG (e.g. mafic-hosted, felsic-hosted, young, back-arc basin  
624 settings (Herzig and Hannington, 1995)), further increasing the potential for environmental impact.

625  
626 Finally, it is widely accepted that Fe-oxidising bacteria play a significant role during the weathering (oxidative  
627 dissolution) of seafloor sulphide ore deposits (Edwards et al., 2003). Rimstidt (1994), Plumlee et al. (1999),  
628 Corkhill (2008) and Koski et al. (2008), all suggest that redox reactions utilising Fe<sup>3+</sup> produced by bacteria catalyse  
629 reaction rates of sphalerite, chalcopyrite, enargite and arsenopyrite. Lizama and Suzuki (1991), show that  
630 *Thiobacillus ferrooxidans* and *Thiobacillus thiooxidans* both increase the leaching rates from sulphide minerals  
631 (pyrite, chalcopyrite, sphalerite) by up to 44.2% in some cases. It has also been reported in numerous dissolution  
632 studies (Ahonen et al., 1985; Berry et al., 1978; Jyothi et al., 1989; Mehta and Murr, 1983, 1982, Natarajan, 1988,  
633 1985, Natarajan and Iwasaki, 1983, 1986; Yelloji Rao and Natarajan, 1989) that the presence of bacteria such as  
634 *Thiobacillus ferrooxidans* in a polymetallic sulphide mixture can accelerate galvanic interactions significantly. Whilst  
635 the role of microbes is highly important in the longer-term, in-situ, natural oxidation of seafloor sulphide ore  
636 deposits, it has been suggested that abiotic oxidation rates of sulphide minerals are more relevant to the oxidation  
637 of sulphides during seafloor mining (Bilenker et al., 2016; McBeth et al., 2011). It is postulated that bacterial  
638 colonization of freshly ground mineral surfaces is unlikely under the rapid time spans of mining (<30 minutes based  
639 on mining scenarios outlined by Nautilus Minerals Inc. However biotic oxidation could be of significant concern  
640 once fine sulphide material has settled after initial extraction and dewatering. Leaching of metals has the potential  
641 to continue after material has settled, not only abiotically but also when bacteria colonise the high surface area of  
642 sulphide material that has been exposed due to mining.

643 **7 Conclusions and future directions**

644 Experiments presented here at 1 atm and 12°C with SMS ore samples from TAG, Mid Atlantic Ridge show a  
645 dissolved concentration of metals (primarily Cu and Pb) at the parts per billion range that is not balanced by  
646 oxidation and precipitation over time. Quantifying the extent to which factor such as galvanic coupling, and  
647 mineralogy (and any associated absorption) or even biotic processes contribute to dissolution rates is not possible  
648 within the design of this study, but will need to be assessed in future studies. Nonetheless, the results of this study  
649 clearly demonstrate that the complexity surrounding the leaching of SMS ore needs to be considered and  
650 accounted for in environmental impact predictions. A combination of this study with analysis of the precipitated  
651 oxides would be a first step in advancing our understanding. It is also worth noting the higher pressure involved on  
652 the seabed.  
653

654  
655 The evidence presented here clearly demonstrates that bulk chemistry alone cannot dictate the concentration of  
656 metals leached into seawater. Instead, a combination of mineralogy, absorption processes and/or galvanic effects  
657 must be considered as the primary driving forces behind the type and concentration of metals released and  
658 removed into the water column during SMS mining. As a result, it is imperative that extensive tests with the full  
659 range of ore mineralogy from future prospect sites are undertaken prior to activation of any extraction activities.  
660 Results where only one type of ore are utilised in experiments are applicable to only a particular area of a deposit  
661 and are not ubiquitous. Furthermore, the study highlights that the presence of Fe oxides/oxy-hydroxides within the  
662 deposit prior to mining (likely in the case of an inactive SMS deposit) could be advantageous in reducing the  
663 environmental toxicity associated with mining. The full contribution of galvanic coupling on the leaching of SMS ore  
664 remains unclear and observation of dissolution and oxidation in situ using atomic force microscopy (AFM)  
665 experiments could help to advance our understanding of galvanic couples between specific mineral combinations.  
666

667 In these experimental simulations, dissolved concentrations exceed the 99% protection, ANZECC toxicity  
668 guidelines by 620 times, and would imply the formation of localised toxicity in a stagnant water column. In reality  
669 this concentration will most likely be rapidly diluted by the entrainment of fresh seawater as a result of plume  
670 mixing (during the mining process) and/or deep ocean currents (site specific). Nevertheless, the distance at which  
671 dilution is achieved to meet guidelines is unlikely to be sufficient, indicating either a potential need for ship-board  
672 dilution prior to the return of waste water or a refinement of the mining process. Dilutions required to meet toxicity  
673 guidelines (for Cu and Pb) when mining a deposit like TAG, are less than half of those required for a deposit like



674 Solwara 1 and imply that a deposit such as TAG could pose less of a risk to mine (in terms of leaching and toxicity)  
675 than Solwara 1. However, it should be noted that concentrations will be much higher compared to these  
676 experiments when scaled to more realistic rock-fluid ratios and a finer grain size (< 8 µm) as proposed for seafloor  
677 mining scenarios.

678

679 SMS deposits that contain higher concentrations of Cu and Pb than TAG, as well as other heavy metals in higher  
680 abundance (e.g. mafic-hosted and felsic-hosted (young, back-arc basin) settings (Herzig and Hannington, 1995))  
681 signify an elevated risk of leaching when considering their environmental impact during the mining process  
682 (smaller grain size and higher rock-fluid ratio). This study highlights the importance of further research to predict  
683 and mitigate the effects of imminent SMS mining.

684

685 In order for deep-sea mining to take place in the future, the environmental impact of such an undertaking needs to  
686 be fully understood and demonstrated. Experiments highlighted here and future planned experiments can help  
687 refine the mining processes and minimise detrimental impacts by providing recommendation of grain size fractions  
688 and rock-fluid ratios that can be adopted to reduce any risk of leaching and toxicity. Furthermore, certain types of  
689 deposit or mineralogies can be identified as presenting more or less of a risk. This can ensure minimal leaching  
690 of heavy metals and a reduction of environmental impact.

## 691 **8 Acknowledgements**

692 We would like to thank The Engineering and Physical Sciences Research Council (EPSRC) and Ascension  
693 Holdings Ltd (AHL) for financially supporting this research. We would also like to thank IODP for kindly providing  
694 TAG samples that allowed for this study to take place. A huge thanks to Sven Petersen and Matthias Frische who  
695 provided considerable assistance with collection and processing of LA-ICP-MS data at GEOMAR Helmholtz-  
696 Zentrum für Ozeanforschung, Kiel. Dieter Garbe-Schönberg and Ulrike Westernströer provided much help and  
697 guidance with the digestion and analysis of the TAG samples at the University of Kiel.

## 698 **9 References**

699

- 700 (CLCS), C. on the L. of the C.S., 2016. Oceans and law of the sea, United Nations [WWW Document]. Submissions, through Secr. United Nations, to Comm. Limits  
701 Cont. Shelf, Purs. to Artic. 76, paragraph 8, United Nations Conv. Law Sea 10 December 1982.  
702 (ISA), I.S.A., 2016. Deep seabed minerals contractors [WWW Document]. Int. Seabed Auth.  
703 Abraitis, P., Patrick, R.A.D., Kelsall, G.H., Vaughan, D.J., 2004a. Acid leaching and dissolution of major sulphide ore minerals: processes and galvanic effects in  
704 complex systems. *Mineral. Mag.* 68, 343–351. doi:10.1180/0026461046820191  
705 Abraitis, P., Patrick, R.A.D., Vaughan, D.J., 2004b. Variations in the compositional, textural and electrical properties of natural pyrite: a review. *Int. J. Miner.*  
706 *Process.* 74, 41–59. doi:10.1016/j.minpro.2003.09.002  
707 Acero, P., Cama, J., Ayora, C., Asta, M.P., 2009. Chalcopyrite dissolution rate law from pH 1 to 3. *Geol. Acta* 7, 389–397. doi:10.1344/105.000001444  
708 Ahonen, L., Hiltunen, P., Tuovinen, O., 1985. The role of pyrrhotite and pyrite in the bacterial leaching of chalcopyrite ores, in: Branion, R.M.R., Ebner, H.G. (Eds.),

709 Fundamental and Applied Biohydrometallurgy. Amsterdam, pp. 13–22.

710 Angel, B.M., Apte, S.C., Batley, G.E., Raven, M.D., 2015. Lead solubility in seawater: an experimental study. doi:10.1071/EN15150

711 Berry, V.K., Murr, L.E., Hiskey, J.B., 1978. Galvanic interaction between chalcopyrite and pyrite during bacterial leaching of low-grade waste. Hydrometallurgy 3,

712 309–326. doi:10.1016/0304-386X(78)90036-1

713 Bilenker, L., 2011. Abiotic Oxidation Rate of Chalcopyrite in Seawater: Implications for Seafloor Mining. University of California Riverside.

714 Bilenker, L.D., Romano, G.Y., McKibben, M.A., 2016. Kinetics of sulfide mineral oxidation in seawater: Implications for acid generation during in situ mining of

715 seafloor hydrothermal vent deposits. Appl. Geochemistry 75, 20–31. doi:10.1016/j.apgeochem.2016.10.010

716 Bonnissel-Gissingner, P., Alnot, M., Ehrhardt, J.-J., Behra, P., 1998. Surface Oxidation of Pyrite as a Function of pH. Environ. Sci. Technol. 32, 2839–2845.

717 doi:10.1021/es980213c

718 Cheng, X., Iwasaki, I., 1992. Pulp Potential and Its Implications to Sulfide Flotation. Miner. Process. Extr. Metall. Rev. 11, 187–210.

719 doi:10.1080/08827509208914206

720 Cherkashev, G.A., Ivanov, V.N., Bel'tenev, V.I., Lazareva, L.I., Rozhdestvenskaya, I.I., Samovarov, M.L., Poroshina, I.M., Sergeev, M.B., Stepanova, T. V.,

721 Dobretsova, I.G., Kuznetsov, V.Y., 2013. Massive sulfide ores of the northern equatorial Mid-Atlantic Ridge. Oceanology 53, 607–619.

722 doi:10.1134/S0001437013050032

723 Constantin, C.A., Chiriță, P., 2013. Oxidative dissolution of pyrite in acidic media. J. Appl. Electrochem. 43, 659–666. doi:10.1007/s10800-013-0557-y

724 Corkhill, C.L., 2008. The mineralogical and biogeochemical transformations associated with As-bearing sulphide minerals in acid mine drainage system. The

725 University of Manchester.

726 Descostes, M., Vitorge, P., Beaucaire, C., 2004. Pyrite dissolution in acidic media. Geochim. Cosmochim. Acta 68, 4559–4569. doi:10.1016/j.gca.2004.04.012

727 ECORYS, 2014. Study to investigate state of knowledge of deep sea mining: Final report: Annex 5 Ongoing and planned activity.

728 Edwards, K.J., 2004a. Special Paper 379: Sulfur Biogeochemistry - Past and Present, Geological Society of America Special Papers. Geological Society of

729 America. doi:10.1130/0-8137-2379-5

730 Edwards, K.J., 2004b. Formation and degradation of seafloor hydrothermal sulphide deposits. Geol. Soc. Am. Spec. Pap. 379, 83–96. doi:10.1130/0-8137-2379-

731 5.83

732 Edwards, K.J., McCollom, T.M., Konishi, H., Buseck, P.R., 2003. Seafloor bioalteration of sulfide minerals: results from in situ incubation studies. Geochim.

733 Cosmochim. Acta 67, 2843–2856. doi:10.1016/S0016-7037(03)00089-9

734 Fallon, E.K., Petersen, S., Brooker, R.A., Scott, T.B., 2017. Oxidative dissolution of hydrothermal mixed-sulphide ore: An assessment of current knowledge in

735 relation to seafloor massive sulphide mining. Ore Geol. Rev. 86, 309–337. doi:10.1016/j.oregeorev.2017.02.028

736 Feely, R.A., Lewison, M., Massoth, G.J., Robert-Baldo, G., Lavelle, J.W., Byrne, R.H., Von Damm, K.L., Curl, H.C., 1987. Composition and dissolution of black

737 smoker particulates from active vents on the Juan de Fuca Ridge. J. Geophys. Res. 92, 11347–11363. doi:10.1029/JB092iB11p11347

738 Franklin, N.M., Stauber, J.L., Lim, R.P., 2001. Development of flow cytometry-based algal bioassays for assessing toxicity of copper in natural waters. Environ.

739 Toxicol. Chem. 20, 160–170. doi:10.1002/etc.5620200118

740 Fullston, D., Fornasiero, D., Ralston, J., 1999. Zeta potential study of the oxidation of copper sulfide minerals. Colloids Surfaces A Physicochem. Eng. Asp. 146,

741 113–121. doi:10.1016/S0927-7757(98)00725-0

742 German, C.R., Petersen, S., Hannington, M.D., 2016. Hydrothermal exploration of mid-ocean ridges: Where might the largest sulfide deposits be forming? Chem.

743 Geol. 420, 114–126. doi:10.1016/j.chemgeo.2015.11.006

744 Gilbert, T., King, B., Benfer, N., Terrens, G., 2008. Appendix 12: Modelling the dispersion of the returned water discharge plume from the Solwara 1 seabed mining

745 project, Manus Basin, Papua New Guinea.

746 Gwyther, D., 2008. Environmental Impact Statement, Solwara 1 Project, in: Main Report Coffey Natural Systems. Brisbane.

747 Hannington, M., Herzog, P., Scott, S., Thompson, G., Rona, P., 1991. Comparative mineralogy and geochemistry of gold-bearing sulfide deposits on the mid-ocean

748 ridges. Mar. Geol. 101, 217–248. doi:10.1016/0025-3227(91)90073-D

749 Hannington, M., Jamieson, J., 2011. Estimating the metal content of SMS deposits, in: Oceans. IEEE.

750 Hannington, M.D., de Ronde, C.E.J., Petersen, S., 2005. Modern seafloor tectonics and submarine hydrothermal systems, Economic Geology: One Hundredth

751 Anniversary Volume: 1905-2005. Society of Economic Geologists. doi:10.1029/GM091p0115

752 Hannington, M.D., Jamieson, J., Monecke, T., Petersen, S., 2010. Modern Sea-Floor Massive Sulfides and Base Metal Resources: Toward an Estimate of Global

753 Sea-Floor Massive Sulfide Potential. Soc. Econ. Geol. Spec. Publ. 15 15, 317–338.

754 Heidel, C., Tichomirowa, M., Junghans, M., 2013. Oxygen and sulfur isotope investigations of the oxidation of sulfide mixtures containing pyrite, galena, and

755 sphalerite. Chem. Geol. 342, 29–43. doi:10.1016/j.chemgeo.2013.01.016

756 Herzig, P.M., Hannington, M.D., 1995. Polymetallic massive sulfides at the modern seafloor a review. Ore Geol. Rev. 10, 95–115. doi:10.1016/0169-

757 1368(95)00009-7

758 Humphris, S.E., Herzig, P.M., Miller, D.J., 1996. 158: College Station, TX (Ocean Drilling Program). Proc. ODP, Init. Repts.

759 Humphris, S.E., Herzig, P.M., Miller, D.J., Alt, J.C., Becker, K., Brown, D., Brüggemann, G., Chiba, H., Fouquet, Y., Gemmill, J.B., Guerin, G., Hannington, M.D.,

760 Holm, N.G., Honnorez, J.J., Iturrino, G.J., Knott, R., Ludwig, R., Nakamura, K., Petersen, S., Reysenbach, A.-L., Rona, P.A., Smith, S., Sturz, A.A., Tivey,

761 M.K., Zhao, X., 1995. The internal structure of an active sea-floor massive sulphide deposit. Nature 377, 713–716. doi:10.1038/377713a0

762 Jyothi, N., Sudha, K.N., Natarajan, K.A., 1989. Electrochemical aspects of selective bioleaching of sphalerite and chalcopyrite from mixed sulphides. Int. J. Miner.

763 Process. 27, 189–203. doi:10.1016/0301-7516(89)90064-1

764 Koleini, S.M.J., Jafarian, M., Abdollahy, M., Aghazadeh, V., 2010. Galvanic Leaching of Chalcopyrite in Atmospheric Pressure and Sulfate Media: Kinetic and

765 Surface Studies. Ind. Eng. Chem. Res. 49, 5997–6002. doi:10.1021/ie100017u

766 Koski, R.A., Munk, L., Foster, A.L., Shanks, W.C., Stillings, L.L., 2008. Sulfide oxidation and distribution of metals near abandoned copper mines in coastal

767 environments, Prince William Sound, Alaska, USA. Appl. Geochemistry 23, 227–254. doi:10.1016/j.apgeochem.2007.10.007

768 Kwong, Y.T.J., Swerhorne, G.W., Lawrence, J.R., 2003. Galvanic sulphide oxidation as a metal-leaching mechanism and its environmental implications.

769 Geochemistry Explor. Environ. Anal. 3, 337–343. doi:10.1144/1467-7873/03/013

770 Li, Z., Heping, L., Liping, X., 2006. Galvanic interaction between galena and pyrite in an open system. Chinese J. Geochemistry 25, 230–237.

771 doi:10.1007/BF02840416

772 Liu, Q., Li, H., Zhou, L., 2008. Galvanic interactions between metal sulfide minerals in a flowing system: Implications for mines environmental restoration. Appl.

773 Geochemistry 23, 2316–2323. doi:10.1016/j.apgeochem.2008.02.024

774 Liu, X., Millero, F.J., 2002. The solubility of iron in seawater. Mar. Chem. 77, 43–54. doi:10.1016/S0304-4203(01)00074-3

775 Lizama, H.M., Suzuki, I., 1991. Interaction of chalcopyrite and sphalerite with pyrite during leaching by Thiobacillus ferrooxidans and Thiobacillus thiooxidans. Can.

776 J. Microbiol. 37, 304–311. doi:10.1139/m91-047

777 Majima, H., 1969. How oxidation affects selective flotation of complex sulphide ores. Can. Metall. Q. 8, 269–273.

778 Majuste, D., Ciminelli, V.S.T., Osseo-Asare, K., Dantas, M.S.S., 2012. Quantitative assessment of the effect of pyrite inclusions on chalcopyrite electrochemistry

779 under oxidizing conditions. Hydrometallurgy 113–114, 167–176. doi:10.1016/j.hydromet.2011.12.020

780 Malmström, M., Collin, C., 2004. Sphalerite weathering kinetics: effect of pH and particle size. Proc. 11th Symp. Water-Rock Interact. 1, 849–852.

781 McBeth, J.M., Little, B.J., Ray, R.I., Farrar, K.M., Emerson, D., 2011. Neutrophilic iron-oxidizing "Zetaproteobacteria" and mild steel corrosion in nearshore marine

782 environments. Appl. Environ. Microbiol. 77, 1405–1412. doi:10.1128/AEM.02095-10

783 McKibben, M.A., Barnes, H.L., 1986. Oxidation of pyrite in low temperature acid solutions: Rate laws and surface textures. Geochim. Cosmochim. Acta 50, 1509–

784 1520. doi:10.1016/0016-7037(86)90325-X

785 Mehta, A.P., Murr, L.E., 1983. Fundamental studies of the contribution of galvanic interaction to acid-bacterial leaching of mixed metal sulfides. Hydrometallurgy 9,

786 235–256. doi:10.1016/0304-386X(83)90025-7

787 Mehta, A.P., Murr, L.E., 1982. Kinetic study of sulfide leaching by galvanic interaction between chalcopyrite, pyrite, and sphalerite in the presence of T. ferrooxidans

788 (30°C) and a thermophilic microorganism (55°C). Biotechnol. Bioeng. 24, 919–40. doi:10.1002/bit.260240413

789 Millero, F.J., 2013. Chemical Oceanography, Fourth Edition. CRC Press.

790 Mills, R.A., Elderfield, H., 1995. Rare earth element geochemistry of hydrothermal deposits from the active TAG Mound, 26°N Mid-Atlantic Ridge. Geochim.

791 Cosmochim. Acta 59, 3511–3524.

792 Monecke, T., Petersen, S., Hannington, M.D., Grant, H., Samson, I., 2016. The minor element endowment of modern sea-floor massive sulfide deposits and

793 comparison with deposits hosted in ancient volcanic successions. Rev. Econ. Geol. 18, 245–306.

794 Moses, C.O., Herman, J.S., 1991. Pyrite oxidation at circumneutral pH. Geochim. Cosmochim. Acta 55, 471–482. doi:10.1016/0016-7037(91)90005-P

795 Moses, C.O., Kirk Nordstrom, D., Herman, J.S., Mills, A.L., 1987. Aqueous pyrite oxidation by dissolved oxygen and by ferric iron. *Geochim. Cosmochim. Acta* 51,  
796 1561–1571. doi:10.1016/0016-7037(87)90337-1  
797 Murr, L.E., 2006. Biological issues in materials science and engineering: Interdisciplinarity and the bio-materials paradigm. *JOM* 58, 23–33. doi:10.1007/s11837-  
798 006-0136-3  
799 Natarajan, K., 1988. Electrochemical aspects of bioleaching polysulfide minerals. *Miner. Metall. Process.* 5, 61–65.  
800 Natarajan, K.A., 1985. Microbe-mineral interactions of relevance in the hydrometallurgy of complex sulphides, in: Mehrotra, S.P., Ramachandran, T.R. (Eds.),  
801 *Progress in Metallurgical Research-Fundamental and Applied Aspects*. Tata McGraw Hill, New Delhi, New Delhi, pp. 105–112.  
802 Natarajan, K.A., Iwasaki, I., 1983. Role of Galvanic Interactions in the Bioleaching of Duluth Gabbro Copper-Nickel Sulfides. *Sep. Sci. Technol.* 18, 1095–1111.  
803 doi:10.1080/01496398308059919  
804 Natarajan, K., Iwasaki, I., 1986. Microbe-mineral interactions in the leaching of complex Sulfides, in: Clum, J.A., Haas, L.A. (Eds.), *Microbiological Effects on*  
805 *Metallurgical Processes*. TMS AIME, New York, New York.  
806 Parry, D.L., 2008. Solwara 1 Project Elutriate Report Phase 1 and 2.  
807 Plumlee, G., Logsdon, M., Filipek, L., 1999. The environmental geology of mineral deposits, in: *The Environmental Geochemistry of Mineral Deposits*. Society of  
808 Economic Geologists, pp. 71–116.  
809 Rimstidt, J.D., Chermak, J.A., Gagen, P.M., 1994. Rates of reaction of galena, sphalerite, chalcopyrite, and arsenopyrite with Fe (III) in acidic solutions, in: Alpers,  
810 C.N., Blowes, D.W. (Eds.), *Environmental Geochemistry of Sulfide Oxidation*. American Chemical Society, Washington, DC, pp. 2–13. doi:10.1021/bk-1994-  
811 0550.ch001  
812 Rimstidt, J.D., Newcomb, W.D., 1993. Measurement and analysis of rate data: The rate of reaction of ferric iron with pyrite. *Geochim. Cosmochim. Acta* 57, 1919–  
813 1934. doi:10.1016/0016-7037(93)90084-A  
814 Romano, G.Y., 2012. Kinetics of Pyrrhotite Oxidation in Seawater: Implications for Mining Seafloor Hotspots.  
815 Salmon, S.U., Malmström, M.E., 2006a. Quantification of mineral dissolution rates and applicability of rate laws: Laboratory studies of mill tailings. *Appl.*  
816 *Geochemistry* 21, 269–288. doi:10.1016/j.apgeochem.2005.09.014  
817 Salmon, S.U., Malmström, M.E., 2006b. Quantification of mineral dissolution rates and applicability of rate laws: Laboratory studies of mill tailings. *Appl.*  
818 *Geochemistry* 21, 269–288. doi:10.1016/j.apgeochem.2005.09.014  
819 Schlitzer, R., 2000. Electronic Atlas of WOCE Hydrographic and Tracer Data Now Available. *Eos Trans. AGU* 81.  
820 Simpson, S., Angel, B., Hamilton, I., Spadaro, D., Binet, M., 2007. Water and Sediment Characterisation and Toxicity Assessment for the Solwara 1 Project.  
821 Subrahmanyam, T.V., Forssberg, K.S.E., 1993. Mineral solution-interface chemistry in minerals engineering. *Miner. Eng.* 6, 439–454. doi:10.1016/0892-  
822 6875(93)90173-K  
823 Webber, A.P., Roberts, S., Murton, B.J., Hodgkinson, M.R.S., 2015. Geology, sulfide geochemistry and supercritical venting at the Beebe Hydrothermal Vent Field,  
824 Cayman Trough. *Geochemistry, Geophys. Geosystems* 16, 2661–2678. doi:10.1002/2015GC005879  
825 Weisener, C.G., Smart, R.S.C., Gerson, A.R., 2004. A comparison of the kinetics and mechanism of acid leaching of sphalerite containing low and high  
826 concentrations of iron. *Int. J. Miner. Process.* 74, 239–249. doi:10.1016/j.minpro.2003.12.001  
827 Wohlgemuth-Ueberwasser, C.C., Viljoen, F., Petersen, S., Vorster, C., 2015. Distribution and solubility limits of trace elements in hydrothermal black smoker  
828 sulfides: An in-situ LA-ICP-MS study. *Geochim. Cosmochim. Acta* 159, 16–41. doi:10.1016/j.gca.2015.03.020  
829 Yelloji Rao, M.K., Natarajan, K.A., 1989. Electrochemical effects of mineral-mineral interactions on the flotation of chalcopyrite and sphalerite. *Int. J. Miner. Process.*  
830 27, 279–293. doi:10.1016/0301-7516(89)90069-0  
831

832 **10 Figure Captions**

833 **Figure 1** A galvanic cell occurs when two sulphide minerals with different rest potentials are coupled together in a  
834 solution that acts as an electrolyte (seawater in this case). The mineral with the higher rest potential behaves as a  
835 cathode (e.g. pyrite) and is galvanically protected with the reduction reaction occurring on its surface. The mineral  
836 with the lower rest potential (e.g. chalcopyrite) behaves as an anode and is preferentially dissolved with oxidative  
837 dissolution occurring on its surface. There are a number of potential reduction reactions that occur on the surface  
838 of the cathode depending on the ions available; shown above are the formation of water as well as hydroxides that  
839 can then ultimately form Fe hydroxides/oxy-hydroxides if ferrous Fe is available. Figure adapted from Murr (2006)  
840 and Fallon et al. (2017). Rest potentials of minerals at pH 4 are taken from Majima (1969) and references therein;  
841 quoted where available are rest potentials of minerals at pH 7 in distilled water, taken from Cheng and Iwasaki  
842 (1992).

843 **Figure 2** The location of TAG samples used in this study. TAG-B is located in the TAG-3 area and TAG H and J in  
844 the TAG-4 area. Detailed bathymetric data is overlaid on the map and the inset shows the location of the TAG  
845 hydrothermal field within the context of the Atlantic Ocean. This figure is reproduced from Humphris et al. (1995).

846 **Figure 3** Back-scattered electron (BSE) and reflected light microscopy photographs (PP, plane polarised; XP,  
847 cross polarised) of samples. TAG-B is a heavily oxidised, brecciated sample containing a high abundance of  
848 quartz, largely coated in silica and oxidation products including Fe oxides and Fe oxy-hydroxides (limonite).  
849 Included in this are grains of pyrite and chalcopyrite, with rare sphalerite. TAG-H is dominantly pyrite and  
850 marcasite with sphalerite veinlets and inclusions. TAG-J is similar with major pyrite and marcasite (less marcasite  
851 than TAG-H), however contains major chalcopyrite and no sphalerite. *py*, pyrite; *ccp*, chalcopyrite; *mc*, marcasite;  
852 *sph*, sphalerite; *qtz*, quartz

853 **Figure 4** Reflected light microscope (plane polarised) images of cleaned powders (2.5 - 45 µm). Presence of  
854 inclusions shows their preservation from whole rock sample through the grinding and sieving process. Chalcopyrite  
855 inclusions are observed in pyrite grains of both TAG B (top) and TAG J (bottom). Contacts between pyrite-  
856 chalcopyrite and sphalerite-chalcopyrite in TAG B and covellite-chalcopyrite in TAG-J are also observed. TAG-H  
857 has common sphalerite-pyrite contacts. Whilst inclusions have been identified in grains of the ore powders, no  
858 quantifiable number can be assigned.

859 **Figure 5a, b and c** Cu, Fe and Pb leached over time with all samples. Concentrations have been corrected to  
860 remove initial starting concentrations of Fe, Cu and Pb in seawater and normalised to mass of ore, volume of  
861 seawater used and surface area of each respective sample and are presented in  $\mu\text{mol}/\text{m}^2$ . Shown for reference  
862 are representative maximum solubility's of Cu, Fe and Pb in seawater taken from experimental and calculation  
863 studies (Angel et al., 2015; Franklin et al., 2001; Liu and Millero, 2002). Only Fe exceeds its solubility limit, which is  
864 expected based on the pH of the system and is supported by observations of Fe oxide/oxy-hydroxide precipitation.

865 **Figure 6a, b and c** Cu, Fe and Pb leached over time with all samples. Concentrations have been corrected to  
866 remove initial starting concentrations of Fe, Cu and Pb in seawater and have been normalised to mass of each  
867 respective sample and are presented in ppb. Shown for comparison is elutriate data produced by Nautilus Minerals  
868 for the EIS (Parry, 2008; Simpson et al., 2007). Pink stars are data from an experiment undertaken with  
869 'representative' Fe-rich Solwara 1 ore at 6 °C, particle size of 3.35 mm and a fluid to rock ratio of 25g to 250 mL  
870 (100 g/L) of seawater (Parry, 2008). Cyan crosses are data from an experiment with a Cu-Zn-Pb rich ore at 22 °C,  
871 particle size of <0.25 mm and a fluid to rock ratio of 1.25 g to 125 mL (10 g/L) of seawater (Simpson et al., 2007).  
872 Solid lines represent absolute concentrations and dashed lines represent concentration (ppb) data scaled to 2 g/L  
873 (ore to seawater ratio) for comparison with experiments undertaken in this study. No corrections can be made to  
874 scale EIS concentrations for temperature and grain size in order for comparison with this study.

875 **Figure 7** The dissolved Cu, Fe and Pb shown in experiments from this study as a percentage of the bulk  
876 concentration. Shown for comparison is the dissolved Cu, Fe and Pb as a percentage of the bulk from elutriate  
877 data produced by Nautilus Minerals for the EIS. Hatched bars indicate concentrations that have been corrected to  
878 2 g/L rock to fluid ratio, in line with this study. a) Initial loss of bulk as a %, at the 10-minute sampling interval. b)  
879 Dissolved concentrations as a % of the bulk, taken as an average after the 30-minute sampling interval.

880  
881

882 **Table 1** Sample list with quoted surface area from BET measurements of ground, sieved and cleaned sulphide ore powders (<45µm). Semi  
883 quantitative data (Wt %) are presented based on powder x-ray diffraction of ground, sieved and cleaned sulphide ore powders (<45µm),  
884 dashes indicate either no observation or that the concentration was below the detection limit. Also presented are observations of inclusions  
885 based upon reflected light microscopy and SEM, EDX. Abbreviations used here are *Py* (pyrite), *Mc* (marcasite), *Ccp* (chalcopyrite), *Cv*  
886 (covellite), *Sp* (sphalerite), *Anh* (anhydrite), *Ox* (Fe oxides/oxy-hydroxides) and *qtz* (quartz). Bulk Fe, Cu and Pb concentration determined  
887 by aqua regia digestion with ICP-OES. Detailed method of acid digestion included in Supplementary Material D.

Location	Sample	Surface Area (m <sup>2</sup> /g)	Mineral Abundances (wt %)								Inclusions	Bulk Fe	SD	Bulk Cu	SD	Bulk Pb	SD
			Py	Mc	Ccp	Cv	Sp	Anh	Ox	Qtz		wt%	ppm	ppm	ppm		
TAG-3	TAG-B	1.843	24.4	--	6.2	--	--	--	5.5	63.9	ccp in py, py in ccp	25.8	1.0	43035	5	182.73	6.84
TAG-4	TAG-H	0.552	37.4	42.0	0.9	--	1.2	0.8	--	17.7	sp in py, mc	44.4	3.8	1130	86	107.97	9.12
TAG-4	TAG-J	0.607	83.8	5.9	5.6	1.4	0.6	--	--	2.6	sp, ccp in py	45.3	5.3	36592	4073	164.05	19.20

888

889

890

891

892

893

894

895

896

897

898

899

900

901

902 **Table 2** Average concentration of Fe, Cu and Pb within pyrite, marcasite and sphalerite. Concentrations determined by laser ablation inductively  
 903 coupled mass spectrometry (LA-ICP-MS). N refers to number of analyses. For detailed LA-ICP-MS methodology, please refer to Supplementary  
 904 Material B.

Sample	Phase	N	Fe wt%	Error	Cu ppm	Error	Pb	Error
TAG-B	Pyrite	4	56.90	2.41	461.20	49.83	11.30	0.68
TAG-H	Pyrite	8	54.21	2.07	33.15	3.67	73.34	4.35
TAG-H	Marcasite	8	55.62	1.87	70.75	4.79	113.59	10.58
TAG-H	Sphalerite	3	0.79	0.02	1720.70	28.35	212.00	6.01
TAG-J	Pyrite	6	57.34	2.64	715.30	43.48	217.30	15.90
TAG-J	Marcasite	3	57.31	1.59	77.20	5.75	65.70	5.29

905  
 906  
 907  
 908 **Table 3** Run parameters for experiments conducted in this study. Temperature, oxygen concentration and conductivity are averages of all  
 909 measurements taken over the course of the run. Dissolved oxygen concentrations were held constant across the duration of experiments. The  
 910 error reported is the standard deviation between those values.

Run	T °C	Sample	Size µm	Initial Mass g	Mass lost on probes g	Mass during run g	Average Dissolved Oxygen Concentration mg L <sup>-1</sup>	Initial pH	Final pH	Conductivity mS cm <sup>-1</sup>
16	11.8 +/- 0.6	TAG-B	2.5 - 45	1.0023	0.0382	0.9641	9.4 +/- 0.04	8.05	7.13	37.9 +/- 0.2
18	13.0 +/- 1.4	TAG-H	2.5 - 45	0.5939	0.0378	0.5561	9.8 +/- 0.70	8.91	7.79	36.5 +/- 0.2
19	11.5 +/- 1.0	TAG-J	2.5 - 45	0.9106	0.0682	0.8424	8.96 +/- 0.90	8.4	7.56	38.6 +/- 0.6

911  
 912  
 913  
 914

